

Effect of Yttrium Oxide on the Formation of the Phase Composition and Porous Structure of Titanium Dioxide

A. A. Shutilov^{a,b}, G. A. Zenkovets^{*a,b}, V. Yu. Gavrilov^a, and S. V. Tsybulya^{a,b}

^aBoreskov Institute of Catalysis, Siberian Branch, Russian Academy of Sciences, Novosibirsk, 630090 Russia

^bNovosibirsk State University, Novosibirsk, 630090 Russia

* e-mail: zenk@catalysis.ru

Received January 14, 2010

Abstract—The formation of the structure of TiO_2 (anatase) doped with 1–5 mol % Y_2O_3 is reported. The dopant changes the anatase structure from regular to nanocrystalline. The nanocrystalline structure consists of incoherently intergrown 5- to 7-nm anatase crystallites (500°C) separated by interblock boundaries accommodating yttrium ions. The formation of the nanocrystalline anatase structure stabilizes small anatase crystallites and raises the anatase-to-rutile phase transition temperature above 900°C . Owing to this structure, the developed specific surface area and fine porous texture of yttrium oxide–doped titanium dioxide survive up to higher temperatures than those of undoped titanium dioxide.

DOI: 10.1134/S0023158411010174

Titanium dioxide is an object of intent attention of researchers because it is widely used as a support for heterogeneous catalysts for environmental protection from nitrogen oxides [1] and carbon monoxide [2, 3], for photocatalytic oxidation of hazardous organics in air and water [4–6], and for partial oxidation of substrates into valuable organic compounds [7, 8]. It is also employed in materials converting solar energy into electricity [9] and in chemical sensors [10]. Titanium dioxide used in nearly all of these applications is anatase with a high degree of dispersion, a large specific surface area, and a porous structure. However, the pure anatase phase is metastable. As the temperature is raised, anatase turns to rutile, and this is accompanied by a change in its crystal structure, by a dramatic decrease in dispersion and in the specific surface area, by a transformation of the porous structure, and by a marked degradation of the properties of the titanium dioxide–based catalyst [3, 11].

Therefore, knowledge of the factors stabilizing the anatase phase of TiO_2 is quite essential for developing new, heat-resistant nanomaterials with an anatase structure.

A thermodynamic analysis of the phase stability of nanocrystalline TiO_2 [12, 13] demonstrated that the widespread view that the free energy of rutile is lower than that of anatase is true only for fairly large crystals, while just the reverse is true for nanosized titanium dioxide. As a consequence, the anatase-to-rutile phase transition in nanosized titanium dioxide occurs only when the anatase crystal size reaches a certain critical value. This critical size is about 14 nm [12], so, for titanium dioxide particles smaller than 14 nm, the anatase phase is more stable. As the anatase crystal size

increases, for example, during sintering, the system passes into the normal state, in which the rutile phase is thermodynamically favorable. On the whole, the relevant experimental data confirm these inferences (see, e.g., [11, 14–16]).

Some authors report other critical anatase particle sizes corresponding to the anatase-to-rutile phase transition. For example, the anatase-to-rutile phase transition was observed when the anatase particle size reached ~ 20 nm [15] or even about 40 nm [11, 16]. This might be due to the presence of anionic or cationic microimpurities whose chemical composition depends on the synthetic procedure. The microimpurities can occur both in the anatase crystal structure and on the crystal surface, and this is a factor influencing the free energy of the nanosized anatase and rutile phases. However, the general dependence of the phase transition on the TiO_2 particle size is quite evident in all cases.

Based on the above data, it would be expected that the regular-to-nanocrystalline transition of the anatase structure will exert a significant effect on the thermal stability of the anatase phase in TiO_2 . We indeed observed that anatase doped with cerium dioxide or silicon dioxide changes its structure from regular to nanocrystalline under heating [17, 18]. The nanocrystalline structure is formed by incoherently intergrown anatase crystallites with the formation of interblock boundaries between them. These boundaries are stabilized by cerium ions or thin silicon dioxide interlayers. Owing to this structure, the growth of anatase crystallites is markedly slowed down and they reach their critical size at a higher temperature, thus raising the anatase-to-rutile phase transition temperature.

Table 1. Phase composition of and structural properties of Y_2O_3 -doped TiO_2

Chemical composition, mol %		Calcination temperature, °C	Phase composition		D_{CSD} , nm	Unit cell parameters	
			phase	content, wt %		a , Å	c , Å
100	0	500	anatase	100	20	3.789	9.524
		750	anatase	60	80	3.787	9.524
		900	rutile	40	85	4.599	2.955
		900	rutile	100	90	4.599	2.957
		500	anatase	100	7	3.791	9.520
		750	anatase	100	25	3.789	9.521
99	1	900	anatase	100	40	3.788	9.529
		1000	rutile	—	91	4.592	2.965
			$\text{Y}_2\text{Ti}_2\text{O}_7$	—	—	—	—
		500	anatase	100	6	3.789	9.522
		750	anatase	100	22	3.790	9.521
		900	anatase	~100	40	3.789	9.529
98	2		$\text{Y}_2\text{Ti}_2\text{O}_7$	traces		10.09	
		500	anatase	100	6	3.791	9.519
		750	anatase	100	13	3.791	9.519
		900	anatase	~100	35	3.788	9.527
		1000	rutile	—	100	4.597	2.959
			$\text{Y}_2\text{Ti}_2\text{O}_7$	—	20	10.119	
95	5	500	anatase	100	6	3.791	9.519
		750	anatase	100	13	3.791	9.519
		900	anatase	~100	35	3.788	9.527
			$\text{Y}_2\text{Ti}_2\text{O}_7$	traces	20	10.120	
		1000	rutile	—	80	4.598	2.957
			$\text{Y}_2\text{Ti}_2\text{O}_7$	—	50	10.119	

It was noted [19, 20] that doping of titanium dioxide with yttrium oxide stabilizes the anatase phase at fairly high temperatures; however, the causes of this stabilization were not investigated.

Here, we report the effect of yttrium oxide admixtures in titanium dioxide on the formation of the anatase structure and on the genesis of the porous structure of xerogels during heat treatment in a wide temperature range.

EXPERIMENTAL

Titanium dioxide samples doped with Y_2O_3 (1–5 mol %) were synthesized by incipient-wetness impregnation. Anatase obtained by the industrial sulfuric acid technology [21] was impregnated with an yttrium nitrate solution and was dried in air and then in a dry box at 110°C for 12 h. Thereafter, it was heat-treated in air between 300 and 1000°C for 4 h.

X-ray diffraction patterns were obtained on a URD-63 diffractometer (Germany) using monochromated $\text{Cu}K\alpha$ radiation (point scanning, $2\theta = 10^\circ$ – 60° , 0.05° increments, counting time of 10 s per point). The coherent-scattering domain size for anatase

(D_{CSD}) was derived from the half-widths of the diffraction peaks of anatase (200), rutile (110) and $\text{Y}_2\text{Ti}_2\text{O}_7$ (222) using the Scherrer formula [22]. The unit cell parameters of anatase were refined by least squares involving all of the observed (seven) reflections, using the POLIKRISTALL program [23]. The error in the determination of the unit cell parameter was $\pm 0.003 \text{ \AA}$.

Transmission electron microscopic images were obtained on a JEM-2010 microscope (Japan) with 1.4 Å resolution at an accelerating voltage of 200 kV. Elemental (EDX) analyses were made using a microanalytical attachment with an EDAX DX-4 energy-dispersive X-ray detector (Ametek Inc., United States). The surface area examined was 150–300 nm². The lowest yttrium detection limit was 0.1 at %.

The specific surface area (S_{BET}) was determined from argon thermal desorption data from four sorption equilibrium points using a SORBI-M device (META, Russia).

The porous structure of materials was studied by low-temperature (77 K) nitrogen sorption using a DigiSorb instrument (Micromeritics, United States). The samples to be examined were pretreated in a vac-

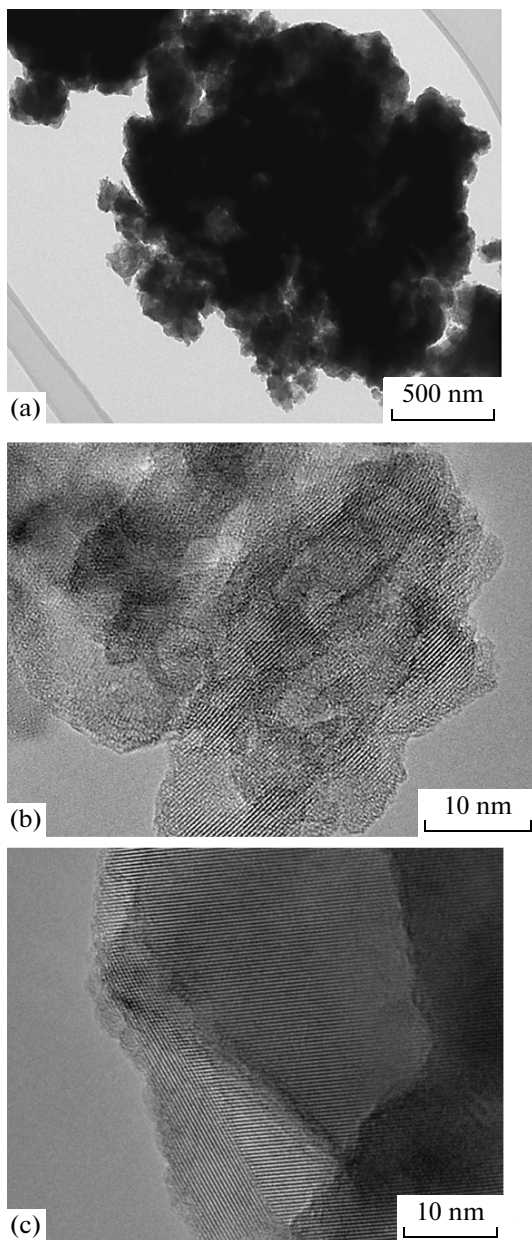


Fig. 1. Electron micrographs of the 2 mol % Y_2O_3 + 98 mol % TiO_2 samples (a) dried at 110°C, (b) calcined at 500°C, and (c) calcined at 900°C.

uum (10^{-4} Torr) at 200°C for 5 h. The mesopore size distribution was derived from the desorption branch of the nitrogen sorption isotherm using the classical Barrett–Joyner–Halenda (BJH) method [24].

RESULTS AND DISCUSSION

Table 1 presents the X-ray diffraction data for yttrium oxide–doped titanium dioxide samples. Clearly, yttrium oxide causes a significant increase in the anatase-to-rutile phase transition temperature. The calcination of doped samples containing 1–5 mol % Y_2O_3 does not

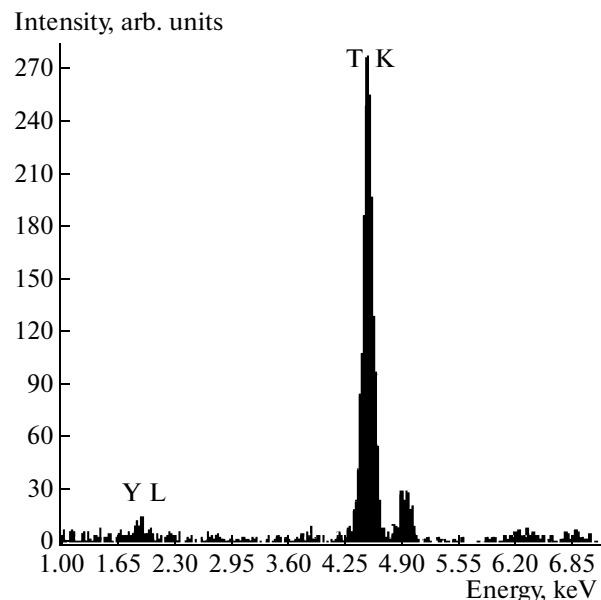


Fig. 2. EDX spectrum of the 2 mol % Y_2O_3 + 98 mol % TiO_2 sample calcined at 500°C.

yield rutile until 900°C, while the rutile phase in undoped titanium dioxide is detectable starting at 750°C. The calcination of the sample containing 5 mol % Y_2O_3 at 900°C yields anatase and traces of the yttrium titanium oxide compound $\text{Y}_2\text{Ti}_2\text{O}_7$, which has a cubic structure (space group $Fd\bar{3}m$) with a unit cell parameter of $a = 10.09 \text{ \AA}$ [25]. In all cases, doped titanium dioxide has a substantially smaller anatase crystallite size (D_{CSD}) than the undoped sample (Table 1). As the yttrium oxide content is raised, D_{CSD} at temperatures of 500 to 900°C decreases. For example, raising the Y_2O_3 content of doped TiO_2 calcined at 750°C from 1 to 5 mol % reduces the D_{CSD} of anatase from 25 to 13 nm. Note that, for undoped anatase calcined at the same temperature, D_{CSD} is about 80 nm.

The unit cell parameters (a and c) of anatase are not changed significantly by doping and coincide with those of the undoped sample ($a = 3.787 \text{ \AA}$, $c = 9.524 \text{ \AA}$) [17]. This suggests that the Y^{3+} ions are not incorporated in the anatase lattice and no anatase-based solution is formed. The ionic radius of Y^{3+} (0.80 Å) is much larger than that of Ti^{4+} (0.64 Å) [26], so if yttrium ions had been incorporated in the anatase structure, there would have been a marked increase in the unit cell parameters of anatase.

As was demonstrated earlier [17], the initial titanium dioxide dried at 110°C consists of fine anatase crystallites loosely packed in larger aggregates up to 1000–1500 nm in size. Electron microscopic data (Fig. 1a) indicate that titanium dioxide doped with yttrium oxide and dried at 110°C is morphologically similar to undoped titanium dioxide and consists of large aggregates of fine anatase crystallites.

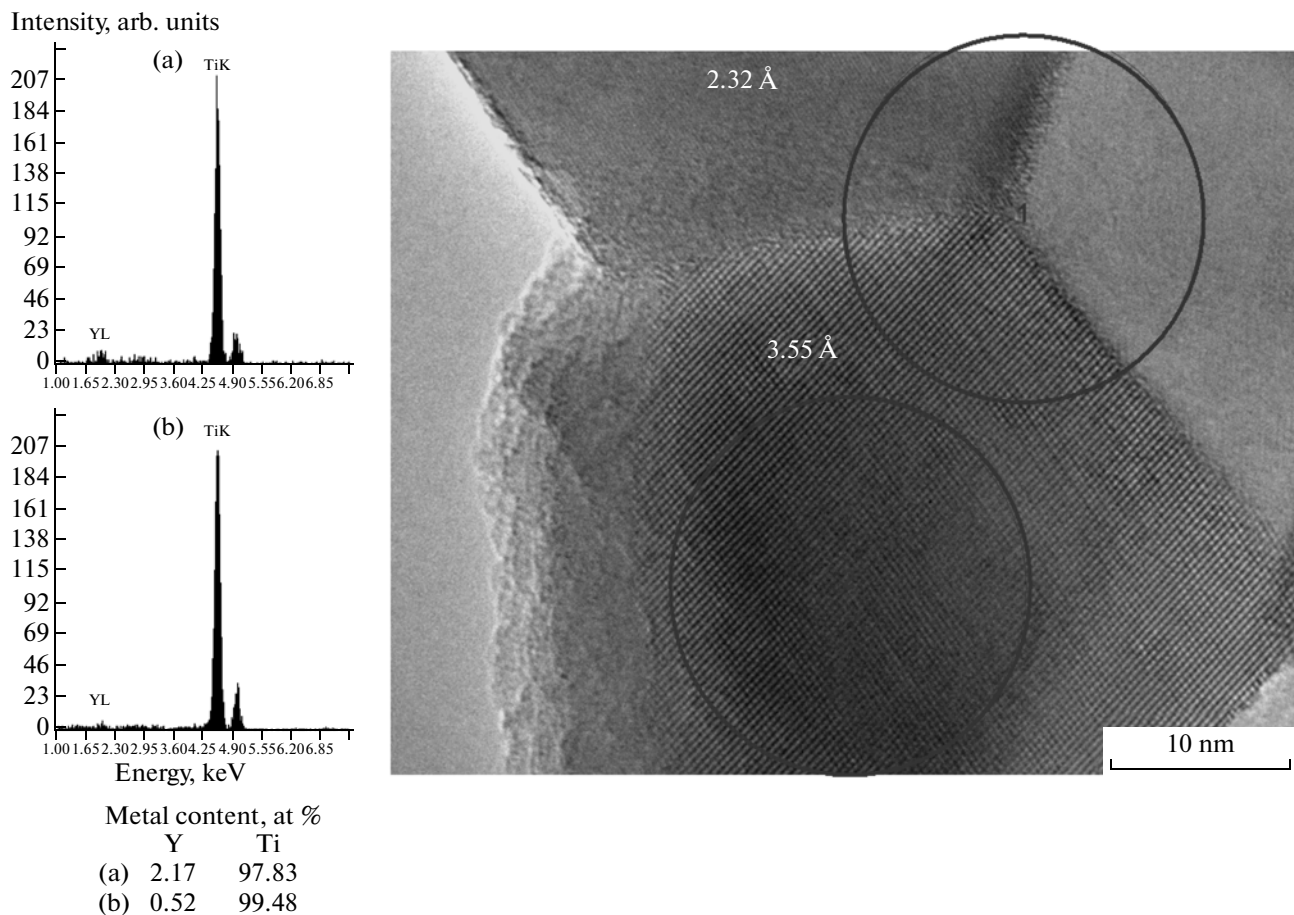


Fig. 3. Electron micrograph of the 2 mol % Y_2O_3 + 98 mol % TiO_2 sample calcined at 900°C and EDX spectra taken from (a) interblock boundaries and (b) regular structure.

The micrograph of the titanium–yttrium sample doped with 2 mol % Y_2O_3 and calcined at 500°C (Fig. 1b) shows that this sample is nanocrystalline, while undoped titanium dioxide calcined at the same temperature has a well-ordered crystal structure [17]. The nanocrystalline structure of doped TiO_2 consists of intergrown fine anatase crystallites 5–7 nm in size separated by interblock (intercrystallite) boundaries. The micrograph shows no other crystalline or amorphous phases. At the same time, microanalysis data indicate that the sample contains yttrium, and the elemental makeup of the sample (1.20 at % Y, 32.34 at % Ti, 66.46 % O) is in agreement with its chemical composition (Fig. 2).

According to electron microscopic data, the same sample calcined at a higher temperature of 750°C has a larger anatase crystallite size of 20–25 nm, retaining its nanocrystalline structure. As the calcination temperature is further raised to 900°C, the nanocrystalline structure of the titanium–yttrium sample persists, but the anatase crystallite size increases to 40 nm, which is in agreement with the D_{CSD} value for anatase (Fig. 1c). Figure 3 shows a micrograph of this sample, in which anatase interblock boundaries are clearly seen. Figure 3

also presents elemental analysis data for the area in which the crystal has a regular structure. The interblock region is substantially richer in yttrium. Therefore, the greater part of the dopant is localized at the interblock boundaries, and this is the main cause of the higher thermal stability and nanocrystallinity of doped anatase at fairly high temperatures.

The micrograph of the 5 mol % Y_2O_3 + 95 mol % TiO_2 sample calcined at 750°C (Fig. 4a) indicates the formation of a nanocrystalline anatase structure in which the crystallite size is smaller (10–15 nm) than the crystallite size in the sample containing 2 mol % Y_2O_3 . These data are in agreement with the X-ray diffraction data (Table 1). Thus, the thermal stability of the interblock boundaries in the nanocrystalline structure of titanium dioxide increases with increasing Y_2O_3 content. The nanocrystalline anatase structure withstands calcination at 900°C, but the anatase particle size increases to 35 nm. In addition, calcination at this temperature leads to the formation of the $\text{Y}_2\text{Ti}_2\text{O}_7$ compound as 15–20 nm crystals mostly intergrown with anatase particles (Fig. 4b).

A comparison between the X-ray diffraction data and the electron microscopic data suggests that most

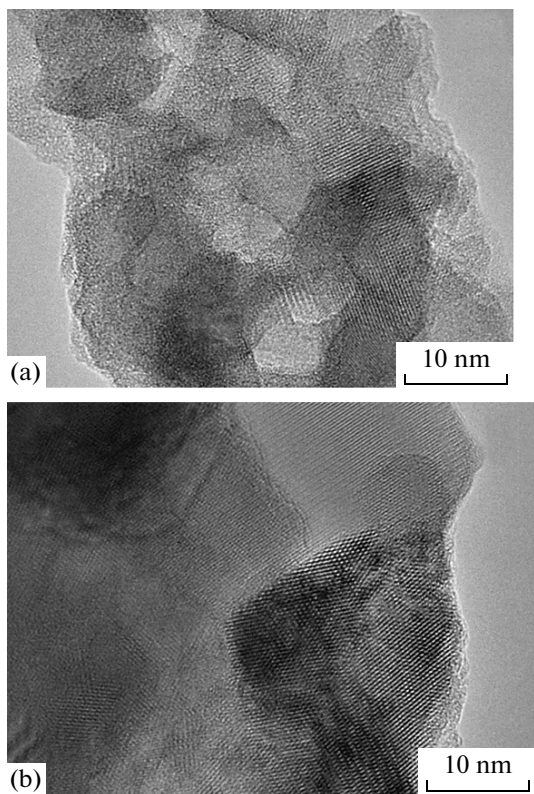


Fig. 4. Electron micrographs of the 5 mol % Y_2O_3 + 95 mol % TiO_2 samples calcined at (a) 750°C and (b) 900°C.

of the Y^{3+} ions in doped anatase are localized at the interblock boundaries formed by intergrown anatase particles, where the anatase structure is heavily disordered. As the yttrium oxide content is increased, the dopant can occupy the anatase particle surface as well, probably as an X-ray-amorphous yttrium–titanium oxide.

The textural characteristics of yttrium oxide-doped titanium dioxide are somewhat different from those of undoped titanium dioxide. The textural characteristics of porous materials are known to be determined by the size and packing density of the primary particles [27]. Figure 5 also shows the micrographs of 5 mol % Y_2O_3 + 95 mol % TiO_2 samples calcined at different temperatures, but these images were obtained at a lower resolution to see the morphology of the particles. The sample calcined at 500°C has irregularly shaped 15- to 30-nm TiO_2 particles consisting of still smaller, intergrown particles. These smaller particles are rather loosely packed into larger aggregates. A similar situation is observed for the sample containing the smaller amount of the dopant. In the 5 mol % Y_2O_3 + 95 mol % TiO_2 sample calcined at 750°C, the TiO_2 particle size is 25–45 nm (mainly 35–45 nm), their complicated structure is retained, and the particle packing in the aggregates is less loose. In the sample calcined at 900°C, the dominant TiO_2 particle size is

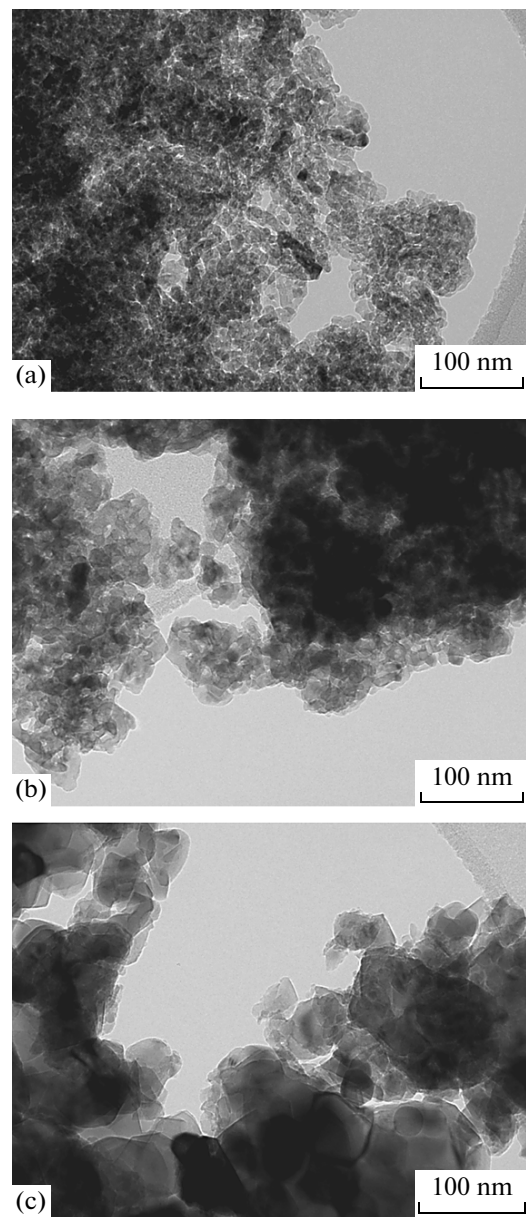


Fig. 5. Electron micrographs of the 5 mol % Y_2O_3 + 95 mol % TiO_2 samples calcined at (a) 500, (b) 750°C, and (c) 900°C, obtained at a lower resolution.

60–70 nm and there are many ~30-nm particles and some particles ≈90 nm in size. Note that the sample remains nanostructured.

Figure 6 demonstrates how the specific surface area of doped titanium dioxide varies with calcination temperature. As the temperature is raised, the S_{BET} of undoped TiO_2 decreases sharply. The specific surface area of doped titanium dioxide also decreases, but less rapidly. For any calcination temperature, the specific surface area of titanium dioxide doped with 1–2 mol % Y_2O_3 is larger than that of undoped TiO_2 . For the sample containing 5 mol % yttrium oxide, S_{BET} is larger than that of undoped TiO_2 only above 400°C. At lower

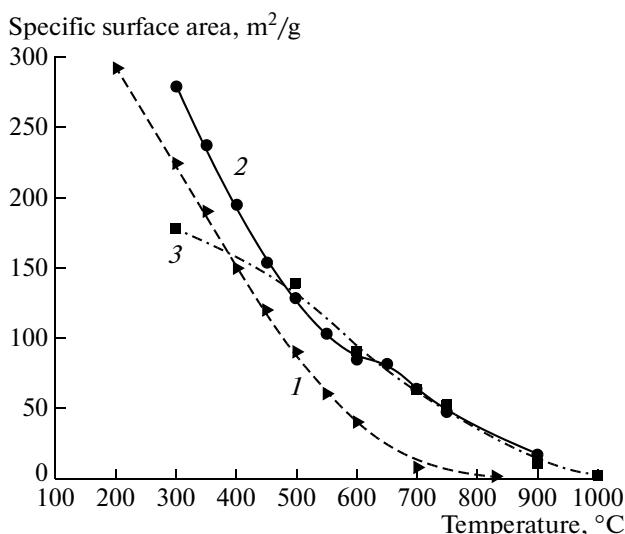


Fig. 6. Effect of the calcination temperature on the specific surface area (1) undoped titanium dioxide and (2, 3) titanium dioxide doped with (2) 2 and (3) 5 mol % Y_2O_3 .

temperatures, this sample has a smaller specific surface area than undoped titanium dioxide. In a wide calcination temperature range (400–900°C), the specific surface area of doped titanium dioxide is practi-

Table 2. Parameters of the porous structure of Y_2O_3 -doped TiO_2

Chemical composition, mol %		Calcination temperature, °C	V_s^* , cm^3/g	D_{pore}^{**} , nm
TiO_2	Y_2O_3			
99	1	300	0.257	3.3
		400	0.264	3.9
		500	0.285	4.7
		600	0.269	7.3
		700	0.287	11.9
	2	300	0.261	3.2
		400	0.278	3.9
		500	0.269	4.8
		600	0.282	7.3
		700	0.282	9.5
95	5	300	0.203	3.1
		400	0.222	3.2
		500	0.208	4.0
		600	0.195	3.8
		700	0.188	4.7

Notes: * Limiting volume of the sorption space, including micropores and mesopores.

** Dominant mesopore diameter.

cally independent of the dopant content. It is possible that the smaller specific surface area of the highly doped sample (5 mol % Y_2O_3) calcined below 400°C is due to the presence of undecomposed yttrium nitrate in the fine pores of the support.

The pore volume (V_s) of the initial TiO_2 support calcined at 300°C is $0.316 \text{ cm}^3/\text{g}$ [28]. It decreases with an increasing dopant content to become $0.203 \text{ cm}^3/\text{g}$ for the sample containing 5 mol % Y_2O_3 (Table 2). The pore volume in all samples increases slightly as the calcination temperature is raised from 300 to 400°C. This can apparently be due to the decomposition of the yttrium salt in the pores of the support. The pore volume in the samples containing 1 and 2 mol % Y_2O_3 is almost unchanged by heat treatment up to 700°C, while the pore volume in the sample containing 5 mol % Y_2O_3 decreases upon heat treatment above 400°C. In addition, experimental data indicate that titanium dioxide containing 5 mol % Y_2O_3 has a substantially smaller pore volume throughout the temperature range examined. This is likely due to the higher TiO_2 particles packing density in the highly doped samples.

Figure 7 shows the differential mesopore size distribution calculated by the BJH method. For the samples containing 1 and 2 mol % Y_2O_3 , raising the calcination temperature to 700°C causes a gradual increase in the dominant pore size (Table 2). For the sample containing 5 mol % Y_2O_3 , raising the calcination temperature to 600°C does not lead to any significant increase in the pore size, which remains at the 3–4 nm level and increases only as the temperature is further increased. For all samples, calcination at 1000°C leads to the total disappearance of the mesopores and diminishes the specific surface area to $2 \text{ m}^2/\text{g}$.

Figure 8 shows how the porous structure of doped titanium dioxide calcined at 600°C depends on the chemical composition of the xerogel. The porous structure of the samples containing 1 and 2 mol % Y_2O_3 is dominated by pores with a uniform diameter of 7.3 nm, and the sample containing 5 mol % Y_2O_3 has a finer porous structure with a dominant pore diameter of 3.8 nm. It is clear from the data presented in Table 2 and Fig. 8 that the persistence of the finer porous texture of the sample containing 5 mol % Y_2O_3 is accompanied by a decrease in the pore volume and is not accompanied by any significant change in the specific surface area. This character of the formation and heat-induced changes of the porous structure of the doped samples suggests that the dopant is partially redistributed, filling some pores and regions of the pore space, as is described by Fenelonov et al. [29]. At low Y_2O_3 concentrations (1–2 mol %), most of the dopant is localized at the boundaries between intergrown fine anatase crystallites, which does not allow a sufficient amount of the surface phase of the dopant to form in the sample. During heat treatment, this causes a gradual increase in the size of the TiO_2 particle without changing their packing density, and this is accompa-

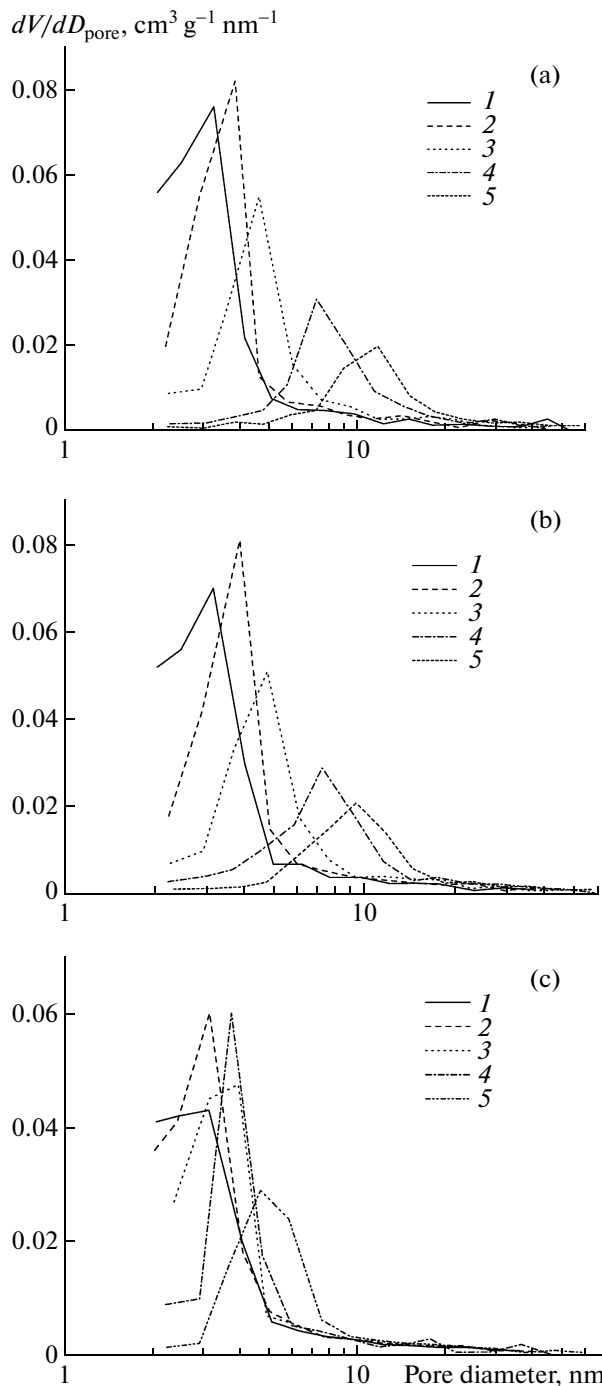


Fig. 7. Differential pore size distribution curves for the samples containing (a) 1, (b) 2, and (c) 5 mol % Y_2O_3 calcined at (1) 300, (2) 400, (3) 500, (4) 600, and (5) 700°C.

nied by a decrease in the specific surface area, by an increase in the dominant pore size, and by no change in the total pore volume. In the highly doped sample (5 mol % Y_2O_3), the dopant is located both at the interblock boundaries and on the outer surface of nanocrystalline TiO_2 particles. This increases the packing density of these particles in their aggregates

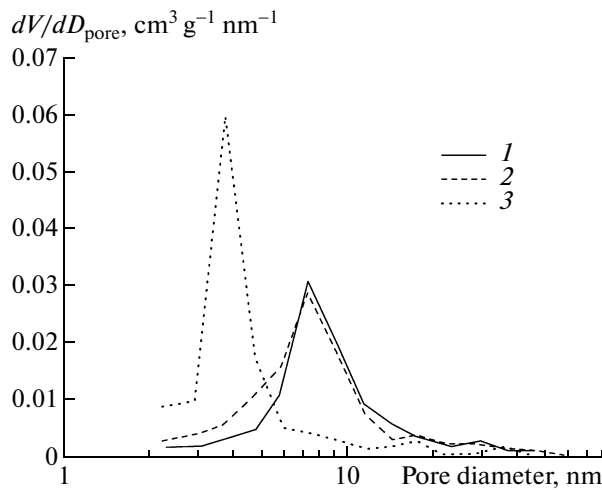


Fig. 8. Differential pore size distribution curves for the samples containing (1) 1, (2) 2, and (3) 5 mol % Y_2O_3 calcined at 600°C.

during heat treatment without reducing the specific surface area and ensures the persistence of the fine porous structure at higher temperatures.

Thus, it follows from our experimental data that, as titanium dioxide is doped with yttrium oxide by impregnation with an aqueous solution of yttrium nitrate, the dopant penetrates into the particle aggregates. Part of the dopant is adsorbed by the surface of anatase particles, and the other part occupies the interparticle space. At the drying and heat treatment stages, the dopant prevents the sintering of the anatase particles. Upon calcination at 500°C, this leads to the formation of a nanocrystalline TiO_2 structure consisting of incoherently intergrown fine anatase crystallites 5–7 nm in size. Interblock boundaries accommodating Y^{3+} ions form between these crystallites. Note that the formation of the nanocrystalline anatase structure occurs only in the presence of the dopant. In the absence of the dopant, the fine anatase crystallites accrete coherently during heat treatment at 500°C to form large crystals with a regular structure.

As was demonstrated in our earlier works [17, 18], the formation of the nanocrystalline anatase structure also takes place in anatase doped with cerium dioxide or silicon dioxide. The thermal stability of the nanocrystalline anatase structure is largely determined by the nature and concentration of the dopant. Doping with cerium and silicon dioxides and, as is demonstrated by this study, yttrium oxide leads to the formation of thermally stable interblock boundaries between anatase crystallites. The formation of these boundaries markedly hampers the growth of the anatase crystallites at high temperatures and, according to [12, 13], raises the anatase-to-rutile phase transition temperature. The anatase phase in the samples containing 1–5 mol % Y_2O_3 is indeed stable up to 900°C, while a

considerable part of anatase in undoped TiO_2 turns into rutile starting at 750°C.

The formation of the porous structure in the binary system is also determined by the increase in the phase transition temperature as a function of the xerogel composition. Note that the decrease in the total pore volume with an increase in the percentage of yttrium oxide is likely due to the dopant occupying pores in the TiO_2 matrix. The thermal stability of the resulting binary structure is confirmed by the finding that the pore volume in the samples containing 1 and 2 mol % Y_2O_3 does not change as the heat treatment temperature is raised to 700°C.

The observation that increasing the amount of dopant at a fixed heat treatment temperature imparts a finer porous texture to the binary system is explained by the fact that the smaller titanium dioxide particles survive at higher Y_2O_3 contents. Accordingly, the mesopore space results from the packing of smaller particles, for which a smaller dominant pore size is typical. The fine porous texture with a pore diameter of $D_{\text{pore}} \approx 4.7$ nm is stable up to 400°C. Thus, the doping of titanium dioxide with yttrium oxide using the procedure suggested here makes it possible to markedly enhance the thermal stability of anatase and to form a heat-resistant fine porous texture at fairly high calcination temperatures.

ACKNOWLEDGMENTS

The authors are grateful to A.V. Ishchenko for carrying out electron microscopic studies.

This work was supported by the Siberian Branch of the Russian Academy of Sciences (interdisciplinary project no. 36) and the Ministry of Education and Science of the Russian Federation through state contract no. P252/23.07.2009 and through the program "Development of the Scientific Potential of the Higher Education Institutions" (project no. 2.1.1/729).

REFERENCES

- Vedrine, J.C., *Catal. Today*, 1994, vol. 20, no. 1, p. 171.
- Alexeev, O.S., Chin, S.Y., Engelhard, M.H., Ortiz-Soto, L., and Amiridis, M.D., *J. Phys. Chem. B*, 2005, vol. 109, no. 49, p. 23 430.
- Shutilov, A.A., Zenkovets, G.A., Kryukova, G.N., Gavrilov, V.Yu., Paukshtis, E.A., Boronin, A.I., Koschcheev, S.V., and Tsybulya, S.V., *Kinet. Katal.*, 2008, vol. 49, no. 2, p. 284 [*Kinet. Catal. (Engl. Transl.)*, vol. 49, no. 2, p. 271].
- Kryukova, G.N., Zenkovets, G.A., Shutilov, A.A., Wilde, M., Gunter, K., Fassler, D., and Richter, K., *Appl. Catal., B*, 2007, vol. 71, no. 3, p. 169.
- Vorontsov, A.V., Savinov, E.N., Barannik, G.D., Troitsky, V.N., and Parmon, V.N., *Catal. Today*, 1997, vol. 38, no. 5, p. 732.
- Photocatalysis: Fundamentals and Applications*, Serpone, N. and Pelizzetti, E., Eds., New York: Wiley, 1989.
- Nicolov, V., Klissurski, D., and Anastasov, A., *Catal. Rev. Sci. Eng.*, 1991, vol. 31, nos. 3–4, p. 319.
- Al'kaeva, E.M., Andrushkevich, T.V., Zenkovets, G.A., Kryukova, G.N., and Tsybulya, S.V., *Catal. Today*, 2000, vol. 61, nos. 1–4, p. 249.
- Park, N.-G., van de Lagemaat, J., and Frank, A.J., *J. Phys. Chem. B*, 2000, vol. 104, no. 38, p. 8989.
- Garzella, C., Comini, E., Tempesti, E., Frigari, C., and Sberveglieri, G., *Sens. Actuators, B*, 2000, vol. 68, p. 189.
- Kholmanov, I.N., Barborini, E., Vinati, S., Piseri, P., Podesta, A., Ducati, C., Lenardi, C., and Milani, P., *Nanotechnology*, 2003, vol. 14, p. 1168.
- Zhang, H. and Banfield, J.F., *J. Mater. Chem.*, 1998, vol. 8, no. 9, p. 2073.
- Kumar, K.P., *Scr. Metall. Mater.*, 1995, vol. 32, p. 873.
- Kim, H.G. and Kim, K.T., *Acta Mater.*, 1999, vol. 47, p. 3561.
- Fu, Y., Gao, W., Xia, T., Zhou, L., and Tian, Y., *Gongneng Cailiao (Chinese)*, 2005, vol. 36, no. 2, p. 250.
- Zenkovets, G.A., Tsybulya, S.V., Burgina, E.B., and Kryukova, G.N., *Kinet. Katal.*, 1999, vol. 40, no. 4, p. 623 [*Kinet. Catal. (Engl. Transl.)*, vol. 40, no. 4, p. 562].
- Zenkovets, G.A., Shutilov, A.A., Gavrilov, V.Yu., Tsybulya, S.V., and Kryukova, G.N., *Kinet. Katal.*, 2007, vol. 48, no. 5, p. 792 [*Kinet. Catal. (Engl. Transl.)*, vol. 48, no. 5, p. 742].
- Zenkovets, G.A., Shutilov, A.A., Gavrilov, V.Yu., and Tsybulya, S.V., *Kinet. Katal.*, 2009, vol. 50, no. 5, p. 790 [*Kinet. Catal. (Engl. Transl.)*, vol. 50, no. 5, p. 760].
- He, X., Chen, R., Zheng, X., and Chen, Z., *Semicond. Photon. Technol.*, 2005, vol. 11, no. 3, p. 192.
- Elaloui, E., Begas, R., Pommier, B., and Pajonk, G.M., *Stud. Surf. Sci. Catal.*, 2002, vol. 143, p. 331.
- Dobrovolskii, I.P., *Khimiya i tekhnologiya oksidnykh soedinenii titana* (Titanium Oxides: Chemistry and Technology), Sverdlovsk: Ural. Otd. Akad. Nauk SSSR, 1988.
- Guinier, A., *Théorie et technique de la radiocristallographie*, Paris: Dunot, 1956.
- Tsybulya, S.V., Cherepanova, S.V., and Solov'eva, L.P., *Zh. Strukt. Khim.*, 1996, vol. 37, no. 2, p. 379.
- Barret, E.P., Joyner, L.G., and Hallenda, P.H., *J. Am. Chem. Soc.*, 1951, vol. 73, no. 1, p. 373.
- Powder Diffraction File no. 42-0413.
- Kataliticheskie svoistva veshchestv: Spravochnik* (Catalytic Properties of Substances: A Handbook), Roiter, V.A., Ed., Kiev: Naukova Dumka, 1968.
- Karnaukhov, A.P., *Adsorbsiya: Tekstura dispersnykh i poristykh materialov* (Adsorption: Texture of Disperse and Porous Materials), Novosibirsk: Nauka, 1999.
- Zenkovets, G.A., Gavrilov, V.Yu., Kryukova, G.N., and Tsybulya, S.V., *Kinet. Katal.*, 1998, vol. 39, no. 1, p. 122 [*Kinet. Catal. (Engl. Transl.)*, vol. 39, no. 1, p. 114].
- Fenelonov, V.B., Tarasova, D.V., and Gavrilov, V.Yu., *Izv. Sib. Otd. Akad. Nauk SSSR, Ser. Khim. Nauk*, 1978, vol. 9, no. 4, p. 116.